1521-0103/391/2/335–345$35.00
THE JOURNAL OF PHARMACOLOGY AND EXPERIMENTAL THERAPEUTICS

dx.doi.org/10.1124/jpet.124.002193
J Pharmacol Exp Ther 391:335–345, November 2024

Nonclinical Profile of PF-06952229 (MDV6058), a Novel TGFβRI/Activin Like Kinase 5 Inhibitor Supports Clinical Evaluation in Cancer[S]

Mausumee Guha, Stephane Thibault, Son Pham, Sebastian Bernales, Rama Pai, Francisco J. Herrera, Theodore R. Johnson, Allison Vitsky, Tina Fernando, and Martin Finkelstein

Pfizer Worldwide Research and Development, La Jolla, California (M.G., S.T., T.R.J., A.V., T.F., M.F.); 1cBio, Inc., Moraga, California (S.P.); Fundación Ciencia & Vida, Santiago, Chile (S.B.); Merck Research Laboratories, South San Francisco, California (R.P.); and Trancura Biosciences, Alameda, California (F.J.H.)

Received February 29, 2024; accepted August 28, 2024

ABSTRACT

The development of transforming growth factor βreceptor inhibitors (TGFβRi) as new medicines has been affected by cardiac valvulopathy and arteriopathy toxicity findings in nonclinical toxicology studies. PF-06952229 (MDV6058) selected using rational drug design is a potent and selective TGFβRI inhibitor with a relatively clean off-target selectivity profile and good pharmacokinetic properties across species. PF-06952229 inhibited clinically translatable phospho-SMAD2 biomarker (≥60%) in human and cynomolgus monkey peripheral blood mononuclear cells, as well as in mouse and rat splenocytes. Using an optimized, intermittent dosing schedule (7-day on/7-day off/cycle; 5 cycles), PF-06952229 demonstrated efficacy in a 63-day syngeneic MC38 colon carcinoma mouse model. In the pivotal repeat-dose toxicity studies (rat and cynomolgus monkey), PF-06952229 on an intermittent dosing schedule (5-day on/5-day off cycle; 5 cycles, 28 doses) showed no cardiac-related adverse findings. However, new toxicity findings related to PF-06952229 included reversible hepatocellular (hepatocyte necrosis with corresponding clinically monitorable transaminase increases) and lung (hemorrhage with mixed cell inflammation) findings at ≥ targeted projected clinical efficacious exposures. Furthermore, partially reversible cartilage hypertrophy (trachea and femur in rat; femur in monkey) and partially to fully reversible, clinically monitorable decreases in serum phosphorus and urinary phosphate at ≥ projected clinically efficacious exposures were observed. Given the integral role of TGFβ in endochondral bone formation, cartilage findings in toxicity studies have been observed with other TGFβRi classes of compounds. The favorable cumulative profile of PF-06952229 in biochemical, pharmacodynamic, pharmacokinetic, and nonclinical studies allowed for its evaluation in cancer patients using the intermittent dosing schedule (7-day on/7-day off) and careful protocol-defined monitoring.

SIGNIFICANCE STATEMENT

Only a few TGFβRi have progressed for clinical evaluation due to adverse cardiac findings in pivotal nonclinical toxicity studies. The potential translations of such findings in patients are of major concern. Using a carefully optimized intermittent dosing schedule, PF-06952229 has demonstrated impressive pharmacological efficacy in the syngeneic MC38 colon carcinoma mouse model. Additionally, a nonclinical toxicology package without cardiovascular liabilities and generally monitorable toxicity profile has been completed. The compound presents an acceptable International Conference on Harmonization of Technical Requirements for Registration of Pharmaceuticals for Human Use S9-compliant profile for the intended-to-treat cancer patients.

The study received no external financial support. The studies included in the manuscript were conducted by Medivation and Pfizer.

No author has an actual or perceived conflict of interest with the contents of this article.

Mausumee Guha, Stephane Thibault, Theodore Johnson, Allison Vitsky, Tinea Fernando, and Martin Finkelstein are Pfizer employees and own company stock. The work has not been presented in any national or international meetings.

An earlier version of this paper appears in "Profile of PF-06952229 (MDV6058), a Novel and Selective TGFβRI/Activin Like Kinase 5 (ALK-5) Inhibitor, Supports Clinical Evaluation in Cancer Patients" under the doi JPET-PI-2024-002115.

dx.doi.org/10.1124/jpet.124.002193.

[S] This article has supplemental material available at jpet.aspetjournals.org.

Introduction

The cytokine transforming growth factor (TGF)β suppresses early stages of carcinogenesis through tumor cell stasis and apoptosis (de Gouville and Huet, 2006; Prud'homme, 2007; Anderton et al., 2011; Colak and Ten Dijke, 2017). In later stages, TGFβ promotes tumor growth through evasion of tumor cell immune surveillance facilitating cancer cell dissemination and metastasis (Bierie and Moses, 2006; Massagué, 2008). Using the canonical signaling pathway (Faivre et al., 2019), TGFβ binds to receptors TGFβRI/activin like kinase (ALK)5 and

ABBREVIATIONS: %TGI, percent tumor growth inhibition; ALK, activin like kinase; CR, complete response; DRF, dose range finding; EMT, epithelial-mesenchymal transition; GLP, Good Laboratory Practices; ICHS9, International Conference on Harmonization of Technical Requirements for Registration of Pharmaceuticals for Human Use S9; IND, investigational new drug; MTV, mean tumor volume; nM, nanomolar; P, phosphorus; PBMC, peripheral blood mononuclear cell; PD, pharmacodynamic; PK, pharmacokinetic; PR, partial response; RBC, red blood cell; SAR, structure–activity relationship; TGFβRi, transforming growth factor β receptor inhibitors; WB, Western blot.

TGFβRII, phosphorylates intracellular signaling proteins (SMAD2 and SMAD3), and activates downstream cascade that supports tumor growth and metastasis (Cheifetz et al., 1987; Akhurst and Hata, 2012). Both tumor intrinsic and indirect tumor extrinsic effects of TGFβ lead to epithelial-mesenchymal transition (EMT). Cancer cells with EMT develop a "stem cell-like" tumor-initiating capacity and drug resistance, blocks host antitumor immune response, and promotes angiogenesis and tumor metastasis (Papageorgis and Stylianopoulos, 2015). The myofibroblastic phenotype promotes increased tumor cell migration, invasion, and cancer progression (Akhurst and Hata, 2012). Therefore, selective inhibition of TGFβRI kinase presents an attractive treatment approach for cancer progression.

Small molecule inhibitors of TGFβRI and dual TGFβRI/RII inhibitors have demonstrated some efficacy in nonclinical tumor models (Uhl et al., 2004; Suzuki et al., 2007; Li et al., 2008). However, compounds have been terminated early in development due to severe cardiovascular findings seen in the nonclinical toxicity studies, thereby presenting a serious clinical liability. Such findings led to the early termination of AZ12601011, AZ12799734 (Anderton et al., 2011), and BMS-986260 (Rak et al., 2020). In female HsdHan:WIST rat, daily dosing with AZ12601011 or AZ12799734 resulted in hemorrhage, inflammation, degeneration, and valvular interstitial cell activation and proliferation (dysplasia/hyperplasia) that were detected in all four heart valves irrespective of dose and duration (Anderton et al., 2011). LY2157299, which is the first TGFβRI/RII dual inhibitor to be tested in cancer patients, also showed adverse cardiovascular as well as severe physeal (femur and sternum) findings in daily, repeat-dose toxicity studies in F344 rat and beagle dogs (Stauber et al., 2014). In contrast to the AZ compounds, the cardiovascular lesions observed with LY2157299 were dose and duration dependent. The findings included degenerative and inflammatory valvular lesions (valvulopathy), myocardial degeneration and necrosis, aortitis with rupture, vasculitis/perivasculitis and correlated increases in heart weights (Stauber et al., 2014)). The Lilly clinical program encountered a "regulatory hold" based on the nonclinical findings that was mitigated by conducting two pivotal 3-month toxicity studies in rat and dog using a modified intermittent dosing schedule (14-day on/14-day off cycle, 3 cycles; 42 dosing days). The drug holiday reduced the cardiovascular toxicity findings and provided sufficient nonclinical exposure margins for the intended clinical exposures. The physeal and cartilage findings, although less severe with intermittent dosing were still detected at lower than target clinical exposures and was attributed to the use of growing animals with open growth plates for toxicity studies (Stauber et al., 2014). Patients who were continued on LY2157299 following the regulatory hold were carefully monitored for potential cardiovascular adverse signals (Herbertz et al., 2015).

To date, the five ALK5i in clinical testing include LY-2157299 (galusertinib), LY-3200882, TEW-7197 (vactosertib), YL-13027, and PF-06952229 (Jin et al., 2014; Herbertz et al., 2015; Kim et al., 2021; Liu et al., 2021; Yap et al., 2021). Galusertinib is being evaluated in metastatic castration-resistant prostate cancer and triple negative breast cancer and has demonstrated overall survival benefits in advanced hepatocellular carcinoma (ClinicalTrials.gov Identifier: NCT02452008) (Herbertz et al., 2015). Vactosertib is in phase 2 evaluations (various combinations) in multiple myeloma, urothelial carcinoma, PD-L1 positive non-small cell lung cancer, metastatic gastric adenocarcinoma, and microsatellite-stable metastatic colorectal cancer (Jung et al., 2020). No cardiac toxicity has been reported to date with these clinical compounds, despite the intense cardiac monitoring and safety biomarker evaluations, (Liu et al., 2021). In the clinic, the compounds have used different intermittent dosing schedules, which are supported by similar schedules used in the pivotal nonclinical toxicity studies.

Herein we describe our efforts to develop and advance PF-06952229, a potent and selective TGFβRI inhibitor (TGFβRIi) for first-in-patient evaluation in cancer. PF-06952229 was designed using careful structure–activity relationships (SAR) optimization (Pujala et al., 2022), and the drug-like properties were confirmed using the cell-based pSMAD2 biomarker and in vitro absorption, distribution, metabolism, and excretion assays. Pharmacokinetic (PK) exposures and efficacy were confirmed in the mice pharmacology studies, safety and toxicokinetic evaluations were completed in rat and cynomolgus monkey, and the off-target profile of PF-06952229 was determined using in vitro CEREP and ion channel secondary pharmacology assays. An investigational new drug (IND)-enabling nonclinical package was completed that supported the progression of PF-06952229 for evaluation in International Conference on Harmonization of Technical Requirements for Registration of Pharmaceuticals for Human Use S9 (ICHS9)-compliant cancer patients.

Materials and Methods

Due to the primary manuscript size limit, additional details are summarized in the Supplemental Materials.

Discovery and Synthesis of PF-06952229. PF-06952229 (MDV6058) was discovered through rational drug design. As described in Pujala et al. (2022), substitution and subsequent optimization of the solvent-exposed region of compound 1 (Discovery lead) improved cellular activity [pharmacodynamic (PD) inhibition of pSMAD2], decreased microsomal clearance in both human and mouse liver microsomes and improved mouse PK. These modifications led to the discovery and selection of PF06952229 as the lead compound for pharmaceutical development. PF-06952229 (free base) was synthesized by Integral Biosciences Pvt. Ltd. (Noida, India) using the method described by Pujala et al., (2022) and US patent 10,030,004 B2. Drug substance (PF-06952229-hydrochloride) for the pivotal [Good Laboratory Practices (GLP)] studies was prepared by Albany Molecular Research, Inc. (New York, NY).

Primary ALK5 Kinase Biochemical Assay for PF-06952229. PF-06952229, LY2157299, and TEW1797 were screened using in vitro biochemical assay for their ability to inhibit the human TGFβRI/ALK5 kinase activity as per the manufacturer's specified protocol (Reaction Biology Corp., Malvern, PA). The assay details are summarized in the Supplemental Materials.

Pharmacodynamic Assessment of pSMAD2 by Western Blot Analysis. PD biomarker assessment for pSMAD2 inhibition in TGFβ-stimulated MDA-MB-231 human breast cancer cell line was conducted in the presence and absence (vehicle) of PF-06952229 using Western blot (WB) analyses. Additional details are included in the Supplemental Materials.

Metabolism and Pharmacokinetic Evaluations. The in vitro metabolic stability of PF-06952229 was evaluated in liver microsomes and hepatocytes from mouse, rat, monkey, and human. Following the addition of PF-06952229 to the in vitro system, aliquots were collected at various time points, and the concentration of PF-06952229 was determined using a quantitative liquid chromatography-tandem mass spectrometry bioanalytical method. Apparent intrinsic clearance values were determined via the rate of depletion of PF-06952229 over time.

The PKs of PF 06952229 were characterized in mice, rats, and monkeys following single-dose intravenous or oral administration. Following PF-06952229 administration, blood samples were collected at various time intervals up to 24 h postdose, and the concentration of PF-06952229 in plasma was determined using a quantitative liquid chromatography-tandem mass spectrometry bioanalytical method. Plasma PK parameters were calculated using standard noncompartmental methods. Details for the in vivo pharmacokinetic and toxicokinetic studies and methods for the determination of PF-96952229 plasma concentrations (mouse, rat, and cynomolgus monkey) are provided in the Supplemental Materials.

Biochemical Potency and Selectivity Confirmation for PF-06952229. The biochemical potency and kinase selectivity of PF-06952229 were determined using a panel of 408 kinases (Thermo Fisher Scientific Invitrogen SelectScreen™, Madison, WI). First the compounds were tested at a concentration of 1 μM (458.9 ng/mL). If the activity was ≥ 50% on any target, a dose–response evaluation was conducted for IC_{50} determination. Additional details for the kinase assay are summarized in the Supplemental Materials.

Secondary Pharmacology Activity of PF-06952229. PF-06952229 was evaluated for off-target activity against a broad panel of receptors, ion channels, transporters, and enzymes (66 targets total) using the CEREP Wide Ligand Profile screen (Eurofins, Panlabs, MO) at a single concentration of 10 μM (4589 ng/mL). Ki or IC_{50} values were determined if inhibition was ≥ 50% in the single-concentration screening for any target. The complete list of targets is presented in the Supplemental Materials.

Pharmacodynamic pSMAD2 Measurements in Splenocytes and Peripheral Blood Mononuclear Cells. A pSMAD2 time course using WB analysis was completed in CD-1 mice splenocytes. CD-1 mice (three mice/time point) were orally dosed with vehicle (two time point spleen collection, 0.5 and 24 h postdose) or PF-06952229 at 10 or 30 mg/kg and spleens were collected (three mice/time point) over a period of 24 h postdose (predose, 0.5, 1, 2, 4, 8, 12, and 24 h) for splenocytes isolation. PF-06952229-mediated percent pSMAD2 inhibition was evaluated over time by densitometric analysis (additional details in the Supplemental Materials). The time course study using the mouse splenocytes is expected to serve as a surrogate for PD target engagement in the tumors and support the outcome of the pharmacology study.

Given that WB assay has low sensitivity and throughput and is not exactly quantitative a clinically translatable sensitive, high-throughput multiplex fluorescent assay was also developed for quantitative PD analysis. This assay was then used to quantitate pSMAD2 inhibition by PF-06952229 in TGFβ1-stimulated MDA-MB-231 cell line, human and cynomolgus monkey peripheral blood mononuclear cells (PBMCs), and mouse and rat splenocytes. Additional details for the PD assay are provided in the Supplemental Materials.

TABLE 1A
Structure and biochemical properties of PF-06952229

Structure	TGFβRI/ ALK5 IC_{50} (μM)[a]	pSMAD2 IC_{50} (μM)[b]
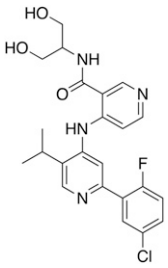	0.024	0.135

[a] IC_{50} (μM) for human ALK5 kinase assay.
[b] PF-06952229 IC_{50} value for TGFβ-dependent phosphorylation of SMAD2 (pSMAD2) in MDA-MB-231 cells using Western blot assay.

Pharmacology Studies. Female C57BL/6 mice bearing established MC38 tumors (mean volume ~100 mm^3) were sorted into four groups (n = 10 mice/group) and dosed by oral gavage with vehicle (group 1, 0.5% methyl cellulose), or PF-06952229 at 10 (group 2) or 30 (group 3) mg/kg twice a day using an intermittent (7-day on/7-day off cycle) schedule and at 30 (group 4) mg/kg twice a day using a daily dosing schedule. Treatment efficacies were determined based on the analysis of mean tumor volume (MTV) and percent tumor growth inhibition (%TGI) on day 18, the last day all evaluable animals were alive in group 1. For percent survival and time to endpoint partial response (PR) or complete response (CR) analyses, the animals were dosed for five cycles and evaluated on the last day of the study (day 63). Additional details on the syngeneic MC38 pharmacology model are provided in the Supplemental Materials.

Toxicology Studies. Choice of toxicology species was based on TGFRI sequence homology (DNA and protein) among the mouse, rat, monkey, and human receptors. The percent sequence identity (ortholog to human) of cynomolgus and rat at the transcript/protein levels were 97 out of 100 and 79 out of 97 (similar for mouse), respectively. In addition, similar pSMAD2 inhibitions (functional assay) were confirmed in human and cynomolgus PBMCs and in mouse and rat splenocytes using the high-throughput, sensitive, fluorescent pSMAD2 assay. Based on the sequence homology, functional assay data, and acceptable PK profile, rat and monkey were selected as the toxicology species for the evaluation of the nonclinical safety profile for PF-06952229. The details of the functional pSMAD2 inhibition assay (PD assay) in rat splenocytes and monkey PBMCs are explained in the pharmacodynamic section, and additional details are included in the Supplemental Materials.

PF-06952229 hydrochloride salt was used for all GLP toxicology studies (Albany Molecular Research, Inc., New York, NY), and the same batch was used to make the drug product for first-in-patient evaluation. All pivotal repeat-dose studies were conducted in compliance with US Food and Drug Administration GLP regulations. All other animal experiments including the exploratory toxicity studies were approved by the Institutional Animal Care and Use Committee and conducted in accordance with the Guide for the Care and Use of Laboratory Animals at Covance Laboratories Inc. Details of the toxicology studies including study design, clinical observations,

TABLE 1B
Kinase selectivity and secondary pharmacology profile

Kinases Tested for IC_{50}	IC_{50} Values (compound, nM)	Repeats (n)
TGFβR1 (ALK5)	0.8 (0.2–4.2)[a]	3
ACVR1B (ALK4)	3.14[b]	1
MAP4K4 (HGK)	4.49	1

CEREP Secondary Pharmacology Screen		Primary Profiling		Follow-up Profiling		
Target with 50% Response in Primary Assay	Assay Format	Test Concentration (μM)	% Inhibition at Test Concentration	Endpoint	Endpoint Value (nM)	Exposure Multiples[b]
GABAA Cl Ch (BZD site)	Binding	10	61	Ki	730	16.6x
PDE4D2	Enzymatic	10	76	IC_{50}	340	7.7x
P38α MAPK	Enzymatic	10	66	IC_{50}	610	13.9x
VEGFR2 kinase	Enzymatic	10	96	IC_{50}	897	20.4x

ACVR1B, activin A receptor type-IB; BZD, benzodiazepine; GABA ClCh, γ-aminobutyric acid chloride channel; MAPK, mitogen-activated protein kinase; PDE4D2, phosphodiesterase 4D2; VEGFR, vascular endothelial growth factor receptor.
[a] 95% geometric confidence interval of 0.2 to 4.2 nM (n = 3) as measured in a LanthaScreen competition binding assay using a recombinant catalytic kinase domain and ATP site targeted fluorescent tracer.
[b] Exposure multiple relative to the predicted unbound C_{max} (44.3 nM) at the projected clinically efficacious dose of 225 mg twice a day, based on efficacious exposure in MC38 nonclinical tumor model.

clinical and microscopic pathology endpoints, and toxicokinetic evaluations are provided in the Supplemental Materials.

Statistical Analysis. For statistical analyses (GraphPad Prism software, version 7.03), group MTVs (used to calculate %TGI) on D18 were compared using one-way ANOVA, followed by Dunnett's posttest. P values of less than 0.05 were considered significant. A Kaplan–Meier survival curve for each treatment group was plotted over a 63-day duration. Median survival (days) was determined for each group, and the hazard ratio (HR) (compared with vehicle) was calculated for each treatment group.

Statistical analysis for hematology and clinical chemistry analyses (repeat-dose toxicity studies) are provided in the Supplemental Materials.

Results

Selection of PF-06952229. PF-06952229 (MDV6058) [4-((2-(5-chloro-2-fluorophenyl)-5-isopropylpyridin-4-yl)amino)-N-(1,3-dihydroxypropan-2-yl)nicotinamide], which was selected following careful SAR optimization from the precursor molecule MDV9086 (Pujala et al., 2022), demonstrated potent TGFβRI/ALK5 inhibition (IC_{50}, 24 nanomolar (nM)] in the primary biochemical screening assay and pSMAD2 PD biomarker inhibition in the TGFβ1-stimulated MDA-MB-231 cells (IC_{50}, 135 nM) by semiquantitative WB analysis (Table 1A).

Kinase Selectivity and Secondary Pharmacology Activities. In the SelectScreen kinase selectivity biochemical assay (Table 1B), which is optimized for each target, PF-06952229 inhibited TGFβRI/ALK5 kinase at an IC_{50} value of 0.8 nM, a potency superior to the original SAR primary screening assay. Other kinases inhibited by PF-06952229 were activin A receptor type-IB (ALK4) and mitogen-activated protein kinase kinase kinase kinase 4 (MAP4K4) (HGK) at IC_{50} values of 3.1 nM and 4.5 nM, respectively. The compound was selective against other TGFβ superfamily receptor kinases, including TGFβRII.

In the off-target secondary pharmacology CEREP screening (Table 1B), PF-06952229 (10 μM) demonstrated activity (response $\geq$ 50%) against four targets in the primary profiling screening assay: γ-aminobutyric acid chloride channel (benzodiazepine binding site), phosphodiesterase 4D2, vascular endothelial growth factor receptor 2, and p38α mitogen-activated protein kinase. In the follow-up assays, K_i and IC_{50} values were generated using concentration curves, and exposure multiples relative to the unbound plasma C_{max} values at the projected clinical efficacious exposure were calculated. The cumulative data from the kinase selectivity and the CEREP screening assays suggest that PF-06952229 is a potent TGFβRIi (over 98.5% selectivity against other human kinases) with a low potential for off-target activities based on the margin multiples at projected clinically efficacious exposures (Table 1B). Activity against other targets was < 50% and is summarized in the Supplemental Materials.

Profile of pSMAD2 Inhibition in Tumor Cell Line, PBMC, and Splenocytes. In the human MDA-MB-231 tumor cell line stimulated with hTGFβ1, the pSMAD2 mean IC_{50} was 46 nM and the calculated unbound IC_{50} was 17 nM (Table 1C). To rationalize the use of mouse in pharmacology studies, as well as rat and cynomolgus monkey in toxicology studies, the total and unbound PF-06952229 IC_{50} values for pSMAD2 inhibition were determined in TGFβ1-stimulated h- and cy-PBMCs and in mouse and rat splenocytes (Table 1C). Inhibition of pSMAD2, which represents a functional clinically translatable PD biomarker of PF-06952229/TGFβRI interaction, was observed across all species tested; average total IC_{50}

TABLE 1C
pSMAD2 inhibition in tumor cell line and in cross-species immune cells

Cell Line	IC_{50} (Total Drug, nM)	IC_{50} (Unbound Drug, nM)[c]
MDA-MB-231	46.09 ± 2.05	17.28 ± 0.77
Species	IC_{50} (Total Drug, nM)	IC_{50} (Unbound Drug, nM)[c]
Human[a]	151.4 ± 20.62	56.78 ± 7.73
Cynomolgus monkey[a]	68.30 ± 3.18	25.61 ± 1.19
Rat[b]	101.65 ± 38.21	38.12 ± 14.33
Mouse[b]	42.91 ± 15.10	16.09 ± 5.66

[a] pSMAD2 inhibition in hTGFβ1 stimulated human or cynomolgus monkey PBMCs.
[b] pSMAD2 inhibition in mTGFβ1 stimulated mouse splenocytes; unbound IC_{50} (IC_{50}u) concentrations were calculated using the formula: IC_{50} = IC_{50} × fu media, where fu media for PF-06952229 is 0.375.

TABLE 2A
Scaled hepatic clearance of PF-06952229 in liver microsomes and hepatocytes

Parameter	Unit	Mouse	Rat	Monkey	Human
Liver microsomes					
$CL_{int,app}$	μL/min/mg	62	43	168	34
$CL_{int,u}$	μL/min/mg	276	236	767	121
CL_b (pred)	mL/min/kg	11	7	13	6
E_h (pred)	%	12%	10%	30%	30%
Hepatocytes					
$CL_{int,app}$	μL/min/M cells	16	9	101	32
$CL_{int,u}$	μL/min/M cells	89	51	414	161
CL_b (pred)	mL/min/kg	10	4	17	7
E_h (pred)	%	11%	6%	39%	35%

CL, clearance; $CL_{int,app}$, apparent intrinsic CL; CL_b (pred), total blood CL scaled from $CL_{int,u}$; $CL_{int,u}$, unbound intrinsic CL; E_h, hepatic extraction ratio.

(unbound IC_{50}) values were 151 (57) nM and 68 (26) nM in h-and cy-PBMC, respectively, and 43 (16) nM and 102 (38) nM in mouse and rat splenocytes, respectively (Table 1C). These data along with the ortholog to human transcript and protein sequence comparisons successfully rationalize the species choices for the pharmacology and toxicology studies.

Profile of PF-06952229 Pharmacokinetic Data Across Nonclinical Species. The in vitro metabolic stability of PF-06952229 was determined across multiple species. The metabolic intrinsic clearance of PF-06952229 in mouse, rat, monkey, and human liver preparations was determined from incubations with liver microsomes and hepatocytes, respectively, and is summarized in Table 2A. Based on in vitro metabolic stability studies, total in vivo clearance of PF-06952229 was predicted to be low in mouse and rat (~10% of liver blood flow) and moderate in monkey and human (~30% to 40% of liver blood flow). Reasonable in vitro to in vivo correlations with human were also confirmed for clearances in mouse and monkey, whereas in vivo clearance was underpredicted in rat.

Profile of PF-06952229 Pharmacokinetic Data Across Nonclinical Species. Single-dose PK studies with PF-06952229 were conducted following intravenous or oral dosing in mice, rats, and monkeys (Table 2B). Following intravenous dosing, PF-06952229 demonstrated moderate plasma clearance (~30% to 45% of liver blood flow) and moderate volume of distribution (~2 to 4 L/kg), resulting in mean half-life values ranging from 1 to 5 h across species. After oral dosing, PF-06952229 exhibited moderate to high oral bioavailability across species. The PK data with PF-0695229 supported the use of mouse for pharmacology studies and rat and monkey for the toxicology studies.

Efficacy of PF-06952229 in a Syngeneic MC38 Murine Colon Cancer Model. The antitumor efficacy of PF-06952229 was evaluated in the syngeneic MC38 colon carcinoma model using female C57BL/6 mice where animals (MTV ~100 mm^3) were dosed by oral gavage with vehicle (group 1, 50% PEG400 in 10 mM citric acid) or PF-06952229 at 10 (group 2) or at 30 mg/kg twice a day, using an intermittent (7-day on/7-day off cycle) schedule (group 3) or a daily schedule (group 4) for up to five cycles (63 days). On day 18 (last day when all animals in group 1 were alive), MTV (mm^3) and %TGI were determined for all groups. The increases in MTV following 18 days of treatment were similar in groups 1 (707 mm^3) and 2 (726 mm^3). Regardless of the dosing schedule, PF-06952229 (30 mg/kg twice a day) significantly inhibited tumor growth (Fig. 1, Table 3) in both group 3 (intermittent, 20 doses, MTV 100 mm^3, %TGI 86) and 4 (daily, 35 doses, MTV 106 mm^3, %TGI 85; $P \leq 0.0001$ vs. vehicle) animals. A Kaplan–Meier survival curve was generated to assess survival over the 63-day study duration (Fig. 2). Like the lack of effect on %TGI, the dosing schedule at 30 mg/kg twice a day (group 3, intermittent vs. group 4, daily) had no effect on median survival (group 3, not defined; group 4, 51 days) or HR (group 3, 0.16; group 4, 0.19) when compared with the vehicle group (Table 3). At 10 mg/kg twice a day (group 2, intermittent), both %TGI on day 18 (–3%) and median survival (26.5 days, HR 0.82) were similar to the vehicle group (Table 3). When inhibition of tumor growth was translated into PR and CR (Table 3), groups 3 (MTV, 100 mm^3; two PRs, four CRs) and 4 (MTV, 100 mm^3; three PRs, one CR) showed significantly improved responses on day 18 compared with groups 1 (MTV, 707 mm^3; no responses) and 2 (MTV, 728 mm^3; one CR). At the end of the study (day 63), PF-0695229-treated mice had 7out of 10 CRs (median survival not reached) in group 3 and 5 out of 10 CRs (median survival 51 days) in group 4, compared with groups 1 and 2 (Table 3).

The efficacy of PF-06952229 in the MC38 model was supported by the pSMAD2 target inhibition time-course data generated in CD1 mice splenocytes, which was considered a surrogate for tumor tissue in the MC38 model. CD-1 mice received a single oral dose of vehicle or PF-06952229 (10 or 30 mg/kg), and spleens were collected over a 24-h period. Splenocytes were prepared (three mice/time point; two time points for vehicle and eight time points for the compound) and assessed by WB analyses (Fig. 3). At 30 mg/kg, the onset of pSMAD2 inhibition was earlier (at 30 min postdose) and qualitatively more robust compared with pSMAD2 inhibition at 10 mg/kg (Fig. 3). The pSMAD2 levels returned to vehicle

TABLE 2B
Pharmacokinetic profile of PF-06952229 in multiple nonclinical species

Species (N)	Dose (mg/kg)	C_{max} (ng/mL)	T_{max} (h)	AUC[a] (ng·h/mL)	CL (mL/min/kg)	V_{ss} (L/kg)	$t_{1/2}$ (h)	F (%)
Mouse	2/IV	—	—	1940	17.2	2.56	1.7	—
(3[b])	10/PO	1230	1	7020	—	—	1.9	73
Rat	2/IV	—	—	1370	24.3	3.46	1.6	—
(4[a])	10/PO	1220	4	7300	—	—	—	109
Monkey	1/IV	—	—	1180	15.1	3.52	3.3	—
(3[a])	5/PO	214	4	1800	—	—	—	40

Em-dash (—) indicates not reported.
AUC, area under the concentration time curve from zero to time of last quantifiable concentration (AUC_t) or infinity (AUC_{inf}); CL, clearance; F, oral bioavailability; IV, intravenous; PO, oral; $t_{1/2}$, half-life (terminal); T_{max}, time of the first occurrence of C_{max}; V_{ss}, volume of distribution.
[a] AUC_{inf} for IV; AUC_t for PO.
[b] Per time point.

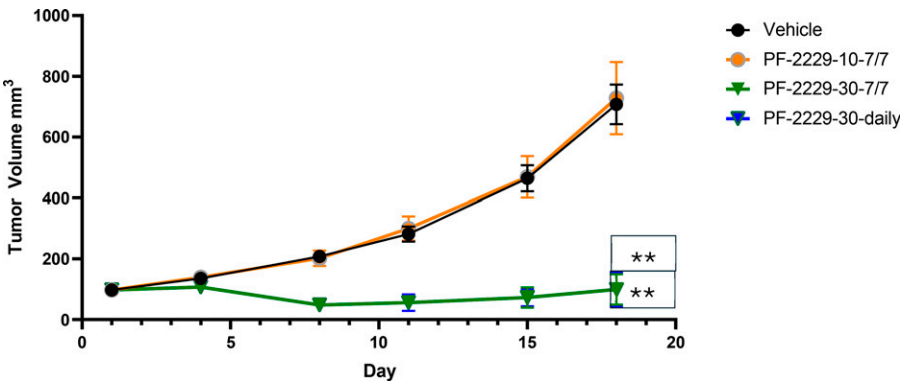

Fig. 1. Effect of various PF-06952229 dosing regimens on in vivo efficacy in the syngeneic MC38 colon carcinoma mouse model. Female C57BL/6 mice bearing established MC38 tumors (mean volume ~100 mm^3) were sorted into four groups (n = 10 mice/group) and dosed by oral gavage with vehicle (group 1, 0.5% methyl cellulose) or PF-06952229 at 10 (group 2) or 30 (group 3) mg/kg twice a day using an intermittent (7-day on/7-day off/cycle) schedule and at 30 (group 4) mg/kg twice a day using a daily dosing schedule. One measure of treatment efficacy was MTV on day 18, the last day all evaluable animals were alive in group 1. The figure shows the progression of MTV over 18 days in the various treatment groups. Data were analyzed using one-way ANOVA followed by Dunnett's multiple comparison test. $^{**}P < 0.001$ compared with MTV in the vehicle group.

control levels by 12 h postdose. The PF-06952229-mediated pSMAD2 inhibition profile at 30 mg/kg in CD-1 mice supported the efficacy data observed in the syngeneic MC38 colon carcinoma model.

Rat and Cynomolgus Monkey Toxicity Studies. The exploratory dose range finding (DRF; non-GLP) studies evaluated various intermittent dosing regimens (doses and schedules) that guided the optimal dose range and dosing schedule (clinically translatable) for the 53-day IND-enabling GLP toxicity studies.

In the rat 12-day DRF study, PF-06952229 was administered at 0, 30 (15 twice a day, low dose), 100/60 (50/30 twice a day, mid dose), or 300 (150 twice a day, high dose) mg/kg/d by oral gavage (details in Supplemental Table 1). On day 3 of dosing, the high dose resulted in mortality and group termination. Dosing in the mid-dose group was also suspended on day 3 due to adverse clinical signs and mortality of two animals (one main study and one toxicokinetic); the remaining animals were given a dosing holiday (2 days) before resuming at 60 mg/kg/d for 12 additional days on an intermittent 5-day on/2-day off/5-day on schedule. There were no clinical signs in the low-dose group during the 12-day repeat dosing other than low carriage on day 12. PF-06952229-related microscopic changes (study end) in the low and revised mid-dose (5-day on/2-day off/5-day on schedule) groups included minimal to slight mixed cell inflammation and hemorrhage in the heart atrioventricular and aortic valves, which occasionally extended into the adjacent proximal aorta; minimal hypertrophy of the physis, minimal to slight decreased resorption of the bone trabeculae of the metaphysis in the femur, and increased liver weights with no microscopic correlate. Clinical pathology differences compared with controls were minor and are presented in Supplemental Table 2. The 12-day DRF study demonstrated that a 5-day on/2-day off/5-day on dosing schedule was not sufficient to mitigate the inflammatory heart valve findings or the physeal changes.

In a second 21-day rat DRF study (7-day on/7-day off/7-day on schedule), PF-06952229 was administered at doses of 0, 20, 40, and 60 mg/kg/d (0, 10, 20, and 30 twice a day) and a fifth group received 20 mg/kg once a day by oral gavage (details of dosing are in the Supplemental Materials). At the end of dosing, PF-06952229-related clinical pathology differences (compared with controls) consisted of lower serum phosphorus (≥0.8x); this finding was attributed to the primary pharmacology of TGFβ in bone physiology. Other clinical pathology findings were minor and are presented in Supplemental Table 3. At ≥ 20 mg/kg twice a day, PF-06952229-related microscopic findings included minimal to mild chondrocyte hypertrophy of epiphyseal plate in the femur, tibia, and fibula, also related to the role of TGFβ in endochondral bone formation. The 7-day on/7-day off/7-day on schedule was clinically well tolerated in rats without any PF-06952229-related severe adverse findings.

In the 53-day pivotal rat GLP study (5-day on/5-day off cycle, 5 cycles + 3 dosing days; 28 total dosing days with 28-day recovery), PF-06952229 was administered at 0, 5, 10, 20, or 40 mg/kg/d (twice a day dosing; details in Supplemental Materials). All doses were clinically tolerated, and there were no adverse clinical or ophthalmologic findings. Key PF-06952229-related hematology differences compared with controls at ≥ 10 mg/kg twice a day included lower red blood cell (RBC) mass parameters (RBC count, hemoglobin, hematocrit, ≥0.95x). Additional PF-06952229-related clinical pathology changes included higher alanine amino transferase

TABLE 3
Summary of pharmacological efficacy of PF-06952229 in MC38 tumor model

Group	N	mg/kg	Dosing Schedule	MTV Day 18	%TGI Day 18	CR Day 63
1	10	NA	Twice daily to the end of the study	707		0
2	9	10	Twice daily 7/7 × 5 (day 1 one dose)	728	−3	1
3	10/9	30	Twice daily 7/7 × 5 (day 1 one dose)	100	86	7
4	10/6	30	Twice daily to end of study	106	85	5

PF-06952229 was orally dosed twice daily on a 7-day on/7-day off cycle for up to five cycles with the first day (day 1) of each cycle receiving one dose (twice daily 7/7 × 5, day 1, one dose), otherwise twice daily to the end of the study.
Day 18 analysis: [(MTV in vehicle – MTV in treatment groups)/MTV in vehicle)] × 100.
Day 63 analysis: criteria for group CR response: tumor volume < 13.5 mm^3 for three consecutive measurements, weight loss < 20%, and treatment-related deaths ≤ 10% during the study.

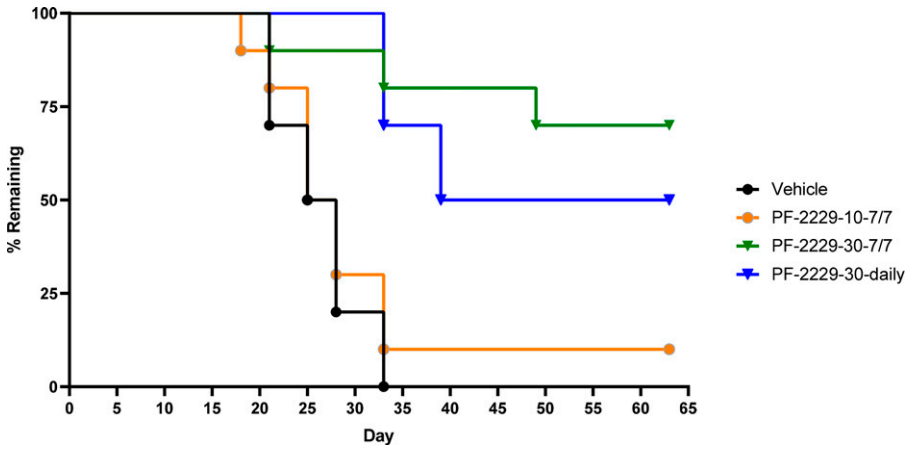

Fig. 2. Effect of various PF-06952229 dosing regimens on survival over 63 days in the syngeneic MC38 colon carcinoma mouse model using the Kaplan–Meier survival curve. Female C57BL/6 mice bearing established MC38 tumors (mean volume ~100 mm^3) were sorted into four groups (n = 10 mice/group) and dosed by oral gavage with vehicle (group 1, 0.5% methyl cellulose) or PF-06952229 at 10 (group 2) or 30 (group 3) mg/kg twice a day using an intermittent (7-day on/7-day off cycle) schedule and at 30 (group 4) mg/kg twice a day using a daily dosing schedule. The figure shows the Kaplan–Meier survival curve (% survival) over 63 days.

activity (≤1.94x) that was accompanied by slight to minimal hepatocellular hemorrhage, necrosis, and mixed cell inflammation in the liver; lower serum calcium (≥0.94x); and reduced serum phosphorus (≥0.85x). The lower serum phosphorus was accompanied by lower urinary phosphorus excretion (≥0.53x) that correlated with a lower urinary phosphorus:creatinine ratio (≥0.56x). The reduction in serum phosphorus was not considered adverse as it was compensated by the lower urinary phosphorus excretion. Regardless, appropriate monitoring was recommended in the clinical protocol. Other clinical pathology findings were minor and are presented in Supplemental Table 4. Microscopic evaluations (Table 4A) demonstrated PF-06952229-related cardiac hypertrophy that was present in the trachea, as well as the articular and physeal cartilages of the femur in both males and females administered 40 mg/kg/d (Fig. 4). This change was still present after a 4-week recovery period. At the 4-week recovery period, one female at 20 mg/kg twice a day had microscopic findings of hemorrhage and focal necrosis in the liver that correlated with severe increases (relative to mean vehicle control) in aspartate aminotransferase and alanine amino transferase (25x and 14x, respectively) although the relationship to PF-06952229 for these changes remain unclear. There were no microscopic findings in the heart or aorta (Fig. 5).

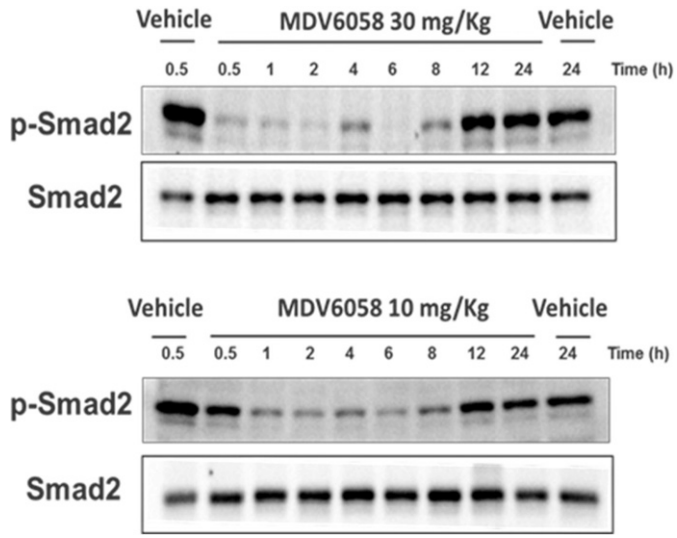

Fig. 3. PF-06952229-mediated target engagement (pSMAD2 inhibition) in CD1 mouse splenocytes. A pSMAD2 time course was determined using WB analysis in CD-1 mice splenocytes. CD-1 mice (three mice/time point) were orally dosed with vehicle (two time point spleen collection, 0.5 and 24 h postdose) or PF-06952229 at 10 or 30 mg/kg and spleens were collected over a period of 24 h (at 0.5, 1, 2, 4, 8, 12, and 24 h) postdose. PF-06952229-mediated pSMAD2 and SMAD2 inhibitions were compared with vehicle-treated control values; pSMAD2 and SMAD levels were determined by densitometry and image quantitation.

In the 12-day cynomolgus monkey DRF (non-GLP) study, PF-06952229 was administered at 0, 60, or 120 mg/kg/d (0, 30, 60 twice a day) on an intermittent 5-day on/2-day off/5-day on schedule or at 0 or 240 mg/kg/d (0, 120 twice a day) on a daily repeat-dose schedule. PF-06952229-related findings included microscopic physeal hypertrophy in the femur at ≥ 60 mg/kg/d and in the sternum at 240 mg/kg/d. Physeal hypertrophy was characterized by expansion of the zone of hypertrophy with an increase in the size and number of chondrocytes. Other findings were limited to clinical pathology and included decreases in RBC mass parameters (RBCs, hematocrit, and hemoglobin; ≥0.8x) with a compensatory increase in reticulocytes (≤5.5x) and decreases in serum phosphorus (≥0.39x) at ≥ 60 mg/kg/d. Additional clinical pathology changes were minor and are listed in Supplemental Table 5. Given the small number of animals studied and intra- and interanimal variability within and between dose groups, conclusions regarding the relationship of clinical pathology changes to PF-06952229 were not definitively determined.

In the 53-day cynomolgus monkey GLP study (5-day on/5-day off per cycle, 5 cycles+ 3 dosing days; 28 total dosing days, 28-day recovery), PF-06952229 was administered at 0, 20, 60, or 200 mg/kg/d (0, 10, 30, and 100 twice a day; details in the Supplemental Materials). There were no PF-06952229-related effects on body weight, ophthalmology, or adverse cardiovascular (electocardiogram) findings in the study, and all doses were clinically tolerated. PF-06952229-related adverse findings (Table 4B) included minimal to mild microscopic physeal hypertrophy in the femurs of males at ≥ 20 mg/kg/d that was characterized by expansion of the zone with an increase in size and number of chondrocytes (Fig. 6); the finding was not reversible at ≥ 60 mg/kg/d at the 4-week recovery period. However, there were no microscopic findings in the heart or aorta (Fig. 7). The bone changes were associated with decreases in serum phosphorus (≥0.61x) and alkaline phosphatase activity (≥0.41x) relative to baseline in both sexes at ≥ 20 mg/kg/d. At ≥ 60 mg/kg/d, there were increases in QTc interval (17–33 milliseconds) on day 3 in males only, a finding not observed in either sex on day 52 (end of dose). Due to the

TABLE 4A
Microscopic findings in rat toxicology studies

	Occurrence of Heart and Cartilage Findings in Rat Studies										
	12-Day DRF (5-2-5)[a]			21-Day DRF (7-7-7)[b]				53-Day GLP Pivotal (5-5) + 3[c]			
AUC μM × h (sex combined mean)	11	15	—	15	31	32	49	10	26	59	142
C_{max} μM (sex combined mean)	4	47	—	2	4	5	5	0.9	2.3	5	12
Dose (mg/kg twice daily)	15	50/30	150[d]	10	20	20[e]	30	2.5	5	10	20
Femur physeal cartilage	√	√			√	√	√			√	√
Femur articular cartilage										√	√
Trachea cartilage				NO	NO	NO	NO				√
Heart valves	√	√	√								
Heart aorta			√								

NO, not observed.
[a] Dosing schedule: 5-day on/2-day off/5-day on.
[b] Dosing schedule: 7-day on/7-day off/7-day on.
[c] Dosing schedule: 5-day on/5-day off + 3 dosing days; 28 total dosing days.
[d] Euthanized on day 3.
[e] Dosed once a day; all doses were administered twice a day unless specified otherwise.
√ Findings were noted.

lack of sustained effect on QTc following longer duration of dosing (day 52), the relationship of the increases on day 3 to PF-06952229 is unclear. Other key, nonadverse PF-06952229-related effects were limited to clinical pathology changes and included decreases in RBC mass parameters (RBC, hematocrit, and hemoglobin; ≥0.82x) and an increase in bilirubin (2.25x) in females at 200 mg/kg/d. All findings exhibited full reversibility following a recovery period of 28 days. Other clinical pathology changes were minor and listed in Supplemental Table 5.

Based on the cumulative data from the toxicology program, PF-06952229 does not present genotoxic or phototoxic liabilities, and no respiratory (rat), neurobehavioral (rat), or cardiovascular (monkey) findings were detected in the single-dose safety pharmacology studies. Based on the findings in the repeat-dose toxicity studies, PF-06952229-related target organ findings included 1) multifocal hepatocellular necrosis (with hemorrhage and mixed cell infiltration) in the liver with associated higher transaminase increases in rat (GLP study) and 2) bone/cartilage hypertrophy/dysplasia with lower in serum phosphorus (P) and urinary phosphate in both species and across studies. In the GLP studies, the clinical pathology changes were partially reversible in rats and fully reversible in monkeys.

Discussion

TGFβ has a role in promoting angiogenesis, tumor invasion, and metastasis through increased EMT and extracellular matrix turnover leading to the remodeling of the tumor microenvironment (Anderton et al., 2011, Massagué, 2008). The cytokine also suppresses the effector T cell response leading to reduced immune surveillance (Bierie and Moses, 2006; Massagué, 2008). Therefore it is encouraging that a few small molecule TGFβRI and TGFβRI/II dual inhibitors have successfully progressed for clinical evaluation in various cancers (Herbertz et al., 2015; Jung et al., 2020; Kim et al., 2021; Yap et al., 2021). Due to the homeostatic role of TGFβ in normal tissues, the potential for cardiotoxicity and severe hyperplastic physeal findings in patients have been addressed by using intermittent dosing regimens that provide sufficient nonclinical to clinical safety margins, based on a lack of microscopic findings using similar regimens in pivotal repeat-dose nonclinical toxicity studies. Examples of intermittent clinical dosing schedules (supported through regulatory interactions) include a 2-week on/2-off cycle with galusertinib (LY2157299) and LY3200882 and a 5-day on/2-day off cycle with vactosertib (Herbertz et al., 2015; Jung et al., 2020; Kim et al., 2021; Yap et al., 2021).

PF-06952229 is a potent and selective TGFβR1i with minimal off-target secondary pharmacology activity; acceptable cross-species PK properties; and no genotoxic, ocular, respiratory, or neurobehavioral toxicity liabilities. The compound has demonstrated good pharmacodynamic activity (pSMAD2 inhibition) in TGFβ-stimulated human (MDA-MB-231) metastatic breast cancer cell line and in TGFβ-stimulated PBMCs

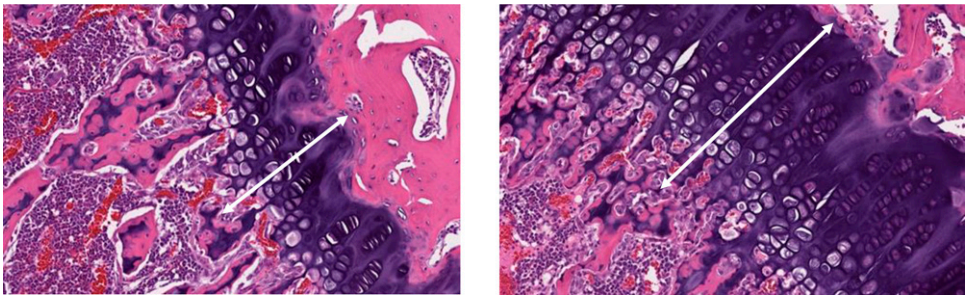

Fig. 4. Representative photomicrographs of the femur physeal cartilage at the end of dose in the GLP rat study. SD rats (both sexes) were dosed with vehicle (left) or PF-06952229 (right, 20 mg/kg twice a day, 40 mg/kg/d) on an intermittent dosing schedule, 5-day on/5-day off cycle (5 cycles + 3 dosing days; 28 dosing days and 25 off days; end of dose on day 53). Hematoxylin and eosin staining of microscopic sections from female rats (also observed in males) demonstrate increased hypertrophy (width of the white arrow) in the femur physeal cartilages for the PF-06952229-treated (right) but not the vehicle-treated animals (10x magnification).

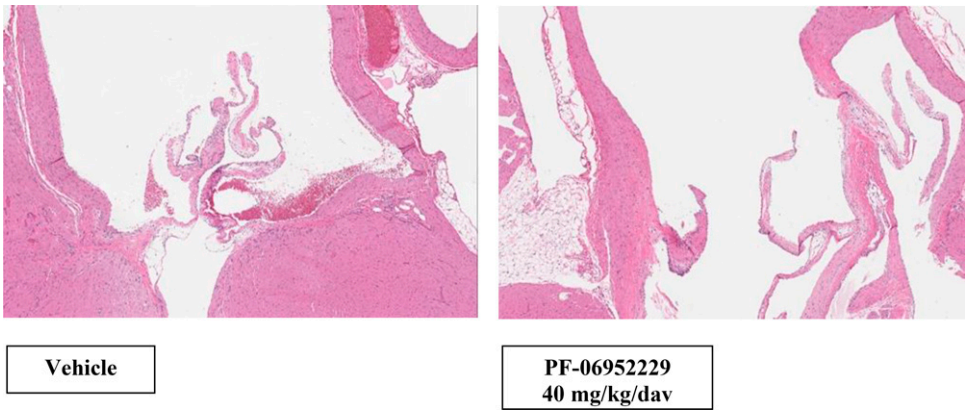

Fig. 5. Representative photomicrographs of the heart and proximal aorta at the end of dose in the GLP rat study. Sprague–Dawley rats (both sexes) were dosed with vehicle (left) or PF-06952229 (right, 20 mg/kg twice a day, 40 mg/kg/d) on an intermittent dosing schedule, 5-day on/5-day off cycle (5 cycles + 3 dosing days; 28 dosing days and 25 off days; end of dose on day 53). Hematoxylin and eosin staining of microscopic sections from the heart and proximal aorta in female rats (similar observation in males) show no adverse findings (valvulopathy or arteriopathy) in the vehicle (left) or PF-06952229-treated (right) rats (2x magnification).

(human and cynomolgus monkey) and splenocytes (mouse and rat). In the syngeneic MC38 colorectal cancer mouse model, PF-06952229 at 30 mg/kg twice a day (compared with vehicle) on an intermittent dosing schedule (7-day on/7-day off cycle, 20 total dosing days) demonstrated significant TGI (86%) on day 18. On day 63, median survival was not reached in this group (HR 0.16 vs. group1), and CR was seen in 7 out of 10 mice. Daily dosing at 30 mg/kg twice a day did not contribute to any additional efficacy when compared with the intermittent schedule group. Therefore, the pharmacology data supported a patient-friendly intermittent dosing schedule (7-day on/7-day off cycle) for clinical evaluation in cancer patients. However, it is important to note that the MC38 pharmacology model used for the evaluation of PF-06952229 is a subcutaneous tumor model generated with a cancer cell line. It is not a model for the development of tumors occurring in colon tissues, and it has limitations due to the differences in vascularization and the tumor microenvironment between implanted subcutaneous tumors and tumors occurring in the original organ or tissue. The pivotal IND-enabling GLP repeat-dose toxicity studies in rat and monkey were conducted on a more stringent (5-day on/5-day off cycle) schedule (5 cycles + 3 days, 28 dosing days; 53 days) with a 28-day postdose recovery period (81-day studies). The schedule used in the pivotal toxicity studies also supported the clinical (7-day on/7-day off cycle) dosing schedule. However, the shorter drug-free days (5 days) in toxicity studies allowed for a more rigorous characterization of the safety profile. PF-06952229-related target organ findings using the 5-day on/5-day off cycle schedule included bone and cartilage hypertrophy in the femur (both species), trachea (rat), and sternum (monkey) as well as physeal dysplasia that was partially reversible in rat but fully reversible in monkey following the recovery period. Additional findings included hepatocellular hemorrhage, necrosis, and mixed cell infiltration in the liver with associated serum transaminase increases (rat only) and decreases in serum and urinary phosphate. No microscopic cardiovascular, aortic, or physeal hyperplastic findings were observed in rat or monkey in the pivotal toxicity studies. Given the role of TGFβ in endochondral bone formation, and that both rat and monkey used in the toxicity studies were growing animals (with open growth plate in bones), the hypertrophic bone and physeal findings with PF-06952229 are an expected pharmacological class effect. However, the translation and risk of the nonclinical physeal findings to similar findings in adult patients, whose bone growths are complete and growth plates are closed (except the sternum), is unclear. Based on the clinical pathology findings in toxicity studies, complete hematology and clinical chemistry monitoring (including serum transaminases and P) are included in patient protocols.

The LY-2157299-related toxicity findings in the daily repeat-dose studies (rat and dog) of ≥ 1-month duration included the cardiovascular, gastrointestinal, immune, musculoskeletal, renal, and reproductive systems (Stauber et al., 2014). The adverse cardiovascular and aortic findings included valve thickening, hemorrhage, and inflammation in the aorta and the arteries; stromal and endothelial hyperplasia; and increased

TABLE 4B
Microscopic findings in cynomolgus monkey toxicology studies

Occurrence of Heart and Cartilage Findings in Monkey Studies												
	12-Day DRF (5-2-5)[a]						53-Day Pivotal (5-5) + 3[b]					
AUC μM × h	34	44	158	1490	165	93	28	17	68	64	243	285
C_{max} μM	4	5	2	11	11	8	3	2	5	5	17	20
Dose (mg/kg twice daily)	30		60		120		10		30		100	
Femur physeal cartilage	NO		NO		NO		√		√		√	
Sternum physeal cartilage	√		√		√		√		√		√	

NO, not observed.
[a] Dosing schedule: 5-day on/2-day off/5-day on.
[b] Dosing duration: 5-day on/5-day off + 3 dosing days, 28 total dosing days, 15 off days; exposures: Male I Female.
√ Findings were noted.

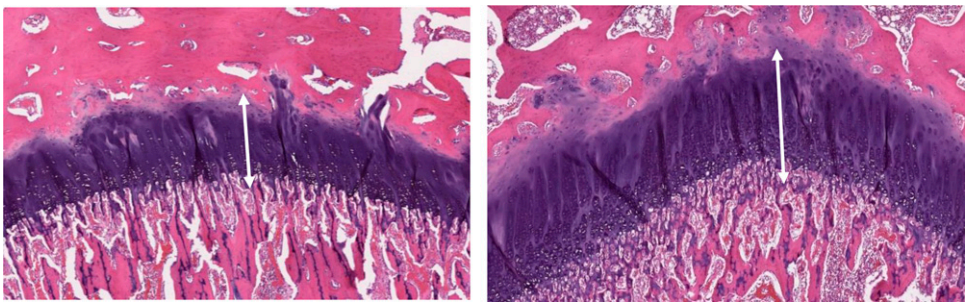

Fig. 6. Representative photomicrographs of the femur physeal cartilage at the end of dose in the GLP cynomolgus monkey study. Cynomolgus monkeys (both sexes) were dosed with vehicle (left) or PF-06952229 (right, 100 mg/kg twice a day, 200 mg/kg/d) on an intermittent dosing schedule, 5-day on/5-day off cycle (5 cycles + 3 dosing days; 28 dosing days and 25 off days; end of dose on day 53). Hematoxylin and eosin staining of microscopic sections from female monkeys (also observed in males) demonstrate increased hypertrophy (width of the white arrow) in the femur physeal cartilages for the PF-06952229-treated (right) but not the vehicle-treated animals (5x magnification).

matrix formation. LY2157299-related skeletal system findings included severe osseous physeal and subphyseal changes in the femur, tibia, and sternum in both rat and dog studies (Stauber et al., 2014). The "regulatory clinical hold" placed on the program particularly due to the nonmonitorable cardiovascular nonclinical findings (≤ 6-month studies) could only be mitigated by changing the daily dosing to an intermittent schedule (14-day on/14-day off cycle). Two 3-month intermittent dosing (42 total dosing days) toxicity studies were conducted in rat and dog to define a no effect level for the cardiac findings. However, the clinical dose of galunisertib (150 mg twice a day) administered using the same intermittent dosing regimen (14-day on/14-day off cycle) translates only to a ~1x no effect level exposure margin for cardiotoxicity (Gueorguieva et al., 2014; Giannelli et al., 2020; Kim et al., 2021). The second Lilly compound LY3200882, which is a more selective TGFβRIi, followed a similar intermittent dosing schedule as LY2157299 (TGFβRI/RII dual inhibitor) in the pivotal toxicity studies (data not available) and in first-in-patient evaluation (Yap et al., 2021). Vacosertib (TEW-7197), another selective TGFβRIi being evaluated in multiple phase 2 trials in cancer patients, uses a different intermittent schedule (5-day on/2-day off cycle) (Jin et al., 2014). In nonclinical toxicity studies in rat and dog, no valvular cardiac or aortic inflammatory findings have been reported with TEW-7197 at the end of the 4-week dosing duration (5-day on/2-day off cycle; 4 cycles; 20 days total dosing) or following the 28-day drug-free recovery period. TEW-7197-related findings included hypertrophy in liver (panlobular) and kidney (tubular), atrophy in ovary, subphyseal hyperostosis, and growth plate thickening in femur and sternum (Jin et al., 2014). The nonclinical findings with LY-2157299 in daily dose toxicity studies, the history of clinical hold, and the mitigation strategy (conducting 3-month intermittent dosing pivotal studies) provided precedence for the pharmaceutical development of PF-06952229 using an intermittent dosing schedule in the nonclinical studies and for clinical evaluation.

Selective TGFβRI inhibitors are expected to provide an improved benefit-risk profile compared with dual TGFβRI/RII inhibitors, although chemotype-specific differences have led to different outcomes in pharmacology and toxicity studies. For example, BMY-986260 is a selective and potent TGFβRIi that has shown tumor growth inhibition only in combination with anti-PD1 antibody but not as a single agent in the same MC38 model in which PF-06952229 was tested (Velaparthi et al., 2020). The pharmacology study used a different intermittent dosing schedule (3-day on/4-day off cycle) for BMY-986260. However, the development of the compound was recently terminated due to adverse valvulopathy and physeal findings as well as mortality in the pivotal 3-month rat (but not the dog) intermittent dosing (3-day on/4-day off cycle; total 36 doses) study (Rak et al., 2020). On the contrary, using a different intermittent dosing schedule (7-day on/7-day off cycle) PF-06952229 has demonstrated single-agent activity (improved %TGI, increased survival and CR) in the MC38 model. Although physeal hypertrophy and minimal dysplasia was observed with PF-06952229 in both rat and monkey in the pivotal studies (28 total doses using the 5-day on/5-day off cycle schedule), the benefit-risk profile of the compound is better than BMY-986260. Therefore, despite being a TGFβRI selective

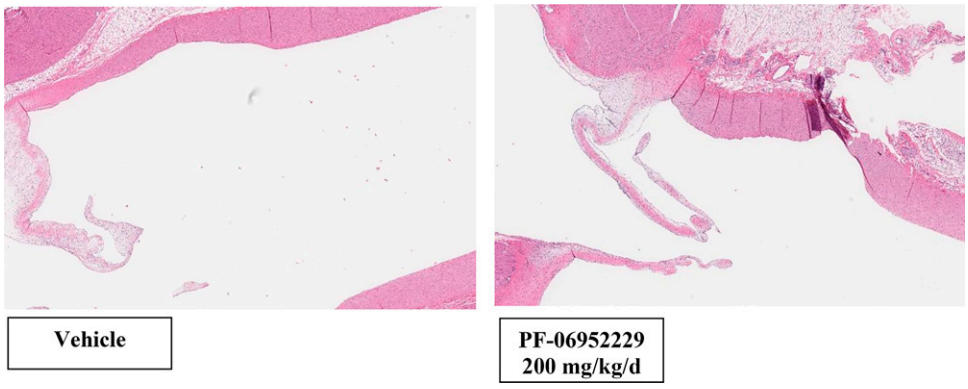

Fig. 7. Representative photomicrographs of the heart and proximal aorta at the end of dose in the GLP Cynomolgus monkeys. Cynomolgus monkeys (both sexes) were dosed with vehicle (left) or PF-06952229 (right, 100 mg/kg twice a day, 200 mg/kg/d) on an intermittent dosing schedule, 5-day on/5-day off cycle (5 cycles + 3 dosing days; 28 dosing days and 25 off days; end of dose on day 53). Hematoxylin and eosin staining of microscopic sections from the heart and proximal aorta in female monkeys (similar observation in males) show no adverse findings (valvulopathy or arteriopathy) in the vehicle (left) or PF-06952229-treated (right) rats (2x magnification).

inhibitor, the chemotype differences appear to contribute to the differential benefit-risk profile of the two compounds.

Of the compounds that have progressed for clinical evaluation, LY-2157299 is a TGFβRI/RII dual inhibitor while TEW-7197 and PF-06952229 are selective TGFβRI inhibitors. However, at the targeted clinical efficacious exposures, the compounds are expected to inhibit a few additional kinases that could contribute to differential benefit-risk profiles in patients. All three compounds are expected to inhibit TNIK and ALK4; additional inhibitions are expected with LY2157299 for MINK1, HGK (MAP4K4), and p38α (MAPK14), with PF-06952229 for MINK1 and with TEW-7197 for vascular endothelial growth factor receptor (R1-R3) (Pfizer internal data; Pujala et al., 2022).

Given the totality of the overall pharmacodynamic, pharmacologic, pharmacokinetic, and toxicity profile and in accordance with the ICHS9 guidance, PF-06952229 was successfully advanced for clinical evaluation (IND) in cancer patients using the optimized intermittent dosing schedule (7-day on/7-day off cycle). Appropriate safety monitoring criteria were built into the protocols for careful dose escalation and dose optimization.

Acknowledgments

The authors would like to thank Kevin Quinn and Jackie Gibbons (Medivation), for the absorption, distribution, metabolism, and excretion and toxicokinetic work, and Robert Lum (Medivation) for coordinating the PF-06952229 drug substance for the pivotal (GLP) studies. They thank Covance Laboratories (Madison, WI) for conducting the toxicology studies and Pfizer Statistician for conducting the statistical analyses, which are presented in the manuscript.

Data Availability

All the data used to support the study's conclusions are included in the Results section in the main manuscript or the Supplemental Materials.

Authorship Contributions

Participated in research design: Guha, Pham, Bernales, Pai, Herrera.

Conducted experiments: Guha, Pham, Bernales, Pai, Herrera.

Contributed new reagents or analytical tools: Guha, Thibault, Bernales, Pai, Herrera, Johnson, Vitsky.

Performed data analysis: Guha, Thibault, Bernales, Pai, Herrera, Johnson, Vitsky.

Wrote or contributed to the writing of the manuscript: Guha, Thibault, Bernales, Pai, Herrera, Johnson, Vitsky, Fernando, Finkelstein.

References

Akhurst RJ and Hata A (2012) Targeting the TGFbeta signalling pathway in disease. *Nat Rev Drug Discov* **11:**790–811.

Anderton MJ, Mellor HR, Bell A, Sadler C, Pass M, Powell S, Steele SJ, Roberts RRA, and Heier A (2011) Induction of heart valve lesions by small-molecule ALK5 inhibitors. *Toxicol Pathol* **39:**916–924.

Bierie B and Moses HL (2006) Tumour microenvironment: TGFbeta: the molecular Jekyll and Hyde of cancer. *Nat Rev Cancer* **6:**506–520.

Cheifetz S, Weatherbee JA, Tsang ML, Anderson JK, Mole JE, Lucas R, and Massagué J (1987) The transforming growth factor-beta system, a complex pattern of cross-reactive ligands and receptors. *Cell* **48:**409–415.

Colak S and Ten Dijke P (2017) Targeting TGF-beta signaling in cancer. *Trends Cancer* **3:**56–71.

de Gouville AC and Huet S (2006) Inhibition of ALK5 as a new approach to treat liver fibrotic diseases. *Drug News Perspect* **19:**85–90.

Elangbam CS (2010) Drug-induced valvulopathy: an update. *Toxicol Pathol* **38:**837–848.

Faivre S, Santoro A, Kelley RK, Gane E, Costentin CE, Gueorguieva I, Smith C, Cleverly A, Lahn MM, Raymond E, et al. (2019) Novel transforming growth factor beta receptor I kinase inhibitor galunisertib (LY2157299) in advanced hepatocellular carcinoma. *Liver Int* **39:**1468–1477.

Giannelli G, Santoro A, Kelley RK, Gane E, Paradis V, Cleverly A, Smith C, Estrem ST, Man M, Wang S, et al. (2020) Biomarkers and overall survival in patients with advanced hepatocellular carcinoma treated with TGF-betaRI inhibitor galunisertib. *PLoS One* **15:**e0222259.

Gueorguieva I, Cleverly AL, Stauber A, Sada Pillay N, Rodon JA, Miles CP, Yingling JM, and Lahn MM (2014) Defining a therapeutic window for the novel TGF-beta inhibitor LY2157299 monohydrate based on a pharmacokinetic/pharmacodynamic model. *Br J Clin Pharmacol* **77:**796–807.

Herbertz S, Sawyer JS, Stauber AJ, Gueorguieva I, Driscoll KE, Estrem ST, Cleverly AL, Desaiah D, Guba SC, Benhadji KA, et al. (2015) Clinical development of galunisertib (LY2157299 monohydrate), a small molecule inhibitor of transforming growth factor-beta signaling pathway. *Drug Des Devel Ther* **9:**4479–4499.

Jin CH, Krishnaiah M, Sreenu D, Subrahmanyam VB, Rao KS, Lee HJ, Park S-J, Park H-J, Lee K, Sheen YY, et al. (2014) Discovery of N-((4-([1,2,4]triazolo[1,5-a]pyridin-6-yl)-5-(6-methylpyridin-2-yl)-1H-imidazol-2 -yl)methyl)-2-fluoroaniline (EW-7197): a highly potent, selective, and orally bioavailable inhibitor of TGF-beta type I receptor kinase as cancer immunotherapeutic/antifibrotic agent. *J Med Chem* **57:**4213–4238.

Jung SY, Hwang S, Clarke JM, Bauer TM, Keedy VL, Lee H, Park N, Kim S-J, and Lee JI (2020) Pharmacokinetic characteristics of vactosertib, a new activin receptor-like kinase 5 inhibitor, in patients with advanced solid tumors in a first-in-human phase 1 study. *Invest New Drugs* **38:**812–820.

Kim B-G, Malek E, Choi SH, Ignatz-Hoover JJ, and Driscoll JJ (2021) Novel therapies emerging in oncology to target the TGF-beta pathway. *J Hematol Oncol* **14:**55.

Li H-Y, McMillen WT, Heap CR, McCann DJ, Yan L, Campbell RM, Mundla SR, King C-HR, Dierks EA, Anderson BD, et al. (2008) Optimization of a dihydropyrrolopyrazole series of transforming growth factor-beta type I receptor kinase domain inhibitors: discovery of an orally bioavailable transforming growth factor-beta receptor type I inhibitor as antitumor agent. *J Med Chem* **51:**2302–2306.

Li W, Li Q, Jiao Y, Qin L, Ali R, Zhou J, Ferruzzi J, Kim RW, Geirsson A, Dietz HC, et al. (2014) Tgfbr2 disruption in postnatal smooth muscle impairs aortic wall homeostasis. *J Clin Invest* **124:**755–767.

Liu S, Ren J, and Ten Dijke P (2021) Targeting TGFbeta signal transduction for cancer therapy. *Signal Transduct Target Ther* **6:**8.

Massagué J (2008) TGFbeta in cancer. *Cell* **134:**215–230.

Papageorgis P and Stylianopoulos T (2015) Role of TGFbeta in regulation of the tumor microenvironment and drug delivery (review). *Int J Oncol* **46:**933–943.

Prud'homme GJ (2007) Pathobiology of transforming growth factor beta in cancer, fibrosis and immunologic disease, and therapeutic considerations. *Lab Invest* **87:**1077–1091.

Pujala B, Ramachandran SA, Sonawane M, Kamble MM, Panpatil D, Adhikari S, Soni S, Subbareddy V, Shinde BU, Nayak AK, et al. (2022) Discovery of MDV6058 (PF-06952229), a selective and potent TGFβR1 inhibitor: design, synthesis and optimization. *Bioorg Med Chem Lett* **75:**128979.

Rak GD, White MR, Augustine-Rauch K, Newsome C, Graziano MJ, and Schulze GE (2020) Intermittent dosing of the transforming growth factor beta receptor 1 inhibitor, BMS-986260, mitigates class-based cardiovascular toxicity in dogs but not rats. *J Appl Toxicol* **40:**931–946.

Stauber A, Credille K, Truex L, Ehlhardt W, and Young J (2014) Nonclinical safety evaluation of a transforming growth factor β receptor I kinase inhibitor in Fischer 344 rats and beagle dogs. *J Clin Toxicol* **4:**1–10.

Suzuki E, Kim S, Cheung H-K, Corbley MJ, Zhang X, Sun L, Shan F, Singh J, Lee W-C, Albelda SM, et al. (2007) A novel small-molecule inhibitor of transforming growth factor beta type I receptor kinase (SM16) inhibits murine mesothelioma tumor growth in vivo and prevents tumor recurrence after surgical resection. *Cancer Res* **67:**2351–2359.

Uhl M, Aulwurm S, Wischhusen J, Weiler M, Ma JY, Almirez R, Mangadu R, Liu Y-W, Platten M, Herrlinger U, et al. (2004) SD-208, a novel transforming growth factor beta receptor I kinase inhibitor, inhibits growth and invasiveness and enhances immunogenicity of murine and human glioma cells in vitro and in vivo. *Cancer Res* **64:**7954–7961.

Velaparthi U, Darne CP, Warrier J, Liu P, Rahaman H, Augustine-Rauch K, Parrish K, Yang Z, Swanson J, Brown J, et al. (2020) Discovery of BMS-986260, a potent, selective, and orally bioavailable TGFbetaR1 inhibitor as an immuno-oncology agent. *ACS Med Chem Lett* **11:**172–178.

Yingling JM, McMillen WT, Yan L, Huang H, Sawyer JS, Graff J, Clawson DK, Britt KS, Anderson BD, Beight DW, et al. (2018) Preclinical assessment of galunisertib (LY2157299 monohydrate), a first-in-class transforming growth factor-beta receptor type I inhibitor. *Oncotarget* **9:**6659–6677.

Yap TA, Vieito M, Baldini C, Sepúlveda-Sánchez JM, Kondo S, Simonelli M, Cosman R, van der Westhuizen A, Atkinson V, Carpentier AF, et al. (2021) First-in-human phase I study of a next-generation, oral, TGFbeta receptor 1 inhibitor, LY3200882, in patients with advanced cancer. *Clin Cancer Res* **27:**6666–6676.

Address correspondence to: Mausumee Guha, 28954 Live Oak Circle, Trabuco Canyon, CA 92679. E-mail: mausumee.guha@yahoo.com